

The Aharonov-Bohm Effect on Quantum Antidot Landau States

N. Aquino,^{1,*} E. Castaño,^{1,†} and E. Ley-Koo^{2,‡}

¹*Departamento de Física, Universidad Autónoma Metropolitana-Iztapalapa,
Apartado Postal 55-534, 09340 México, D.F., México*

²*Instituto de Física UNAM, Apartado Postal 20-364, 01000 México, D.F., México*
(Received December 31, 2002)

A quantum antidot is modeled as an electron moving outside a cylinder of radius a . The charged particle and the geometry of the antidot are elements that also appear in the Aharonov-Bohm effect. This article combines these common physical and geometrical elements of the quantum system and the physical effects of the magnetic vector potential for the analysis of the Aharonov-Bohm effect on quantum antidot Landau states.

PACS numbers: 03.65.Ge, 03.65.Ta, 73.21.La

I. INTRODUCTION

The original Landau states correspond to an electron subject to the action of a uniform magnetic induction field in all points of space; they were constructed in both the linear gauge and the symmetric gauge [1, 2]. Recently, the connection between the eigenstates in the respective gauges has been explicitly identified [3]. Also, the Landau states for an electron confined to move inside an annular cylindrical box and the Aharonov-Bohm effect on such states, produced by the difference between the magnetic induction fields in the perforation and in the interior of the box, were investigated [4].

Advances in microfabrication in the past decades have made available artificial electronic structures in the form of solids of different shapes and increasingly smaller sizes, ranging from the mesoscopic to the nanometric scales [5, 6]. The small size of such structures translates into the quantization of the electron energies, and justifies the names of quantum dots, quantum wires, quantum discs, quantum rings, quantum antidots, etc. The confinement effect on the electrons in such structures has been modeled in two alternative ways: 1) using boxes with impenetrable walls represented by infinitely high potential barriers, such as in [4], and 2) using a harmonic oscillator potential for the confinement in a finite region and the centrifugal potential to exclude the electron from a central region, as in the model of Tan and Inkson [7]. Both models can be solved exactly and include the above mentioned shapes as particular cases; at the same time, both models also allow exact solutions for the Aharonov-Bohm effect.

The geometry of the original theoretical work of Aharonov and Bohm [8] and the experimental implementation by Chambers [9] incorporates the exclusion of the electron from the region where the magnetic flux (i.e. the whisker) is present; it coincides with the geometry of a quantum antidot, or perhaps a better name could be a quantum antiwire.

In section II we define a confined electronic system, the magnetic field configurations for its Landau states and for the Aharonov-Bohm effect on such states; then the respective Schrödinger equations are successively formulated and solved. Section III presents the numerical results for both problems and also a discussion of the connections within the model and with other models, especially those of [4] and [7].

II. QUANTUM ANTIDOTS IN MAGNETIC FIELDS

The model of a quantum antidot to be analyzed in this section consists of an electron which can move everywhere in all space except for an excluded cylindrical region defined by $(0 < \rho < a, \phi, z)$ in cylindrical coordinates. Our purpose is to investigate the quantum states of such an electron in two comparative situations: A) under the action of a uniform magnetic induction field $\vec{B} = \hat{k}B$ throughout space including the excluded region, and B) under the action of the same magnetic induction field in the allowed region with a different uniform magnetic induction field $\vec{B}' = \hat{k}B'$ in the excluded region.

The Hamiltonian, constructed via the minimum coupling prescription, is

$$H = \frac{(\vec{p} + \frac{e}{c}\vec{A})^2}{2m_e}, \quad (1)$$

where \vec{A} is the electromagnetic vector potential. For the situations of interest, the latter takes the respective forms

$$\vec{A}(0 < \rho < \infty, \phi, z) = \frac{1}{2}B\rho\hat{\phi} \quad (2a)$$

and

$$\vec{A}(0 < \rho < a, \phi, z) = \frac{1}{2}B'\rho\hat{\phi}$$

$$\vec{A}(a < \rho < \infty, \phi, z) = \frac{1}{2}\left(B\rho + \frac{(B' - B)a^2}{\rho}\right)\hat{\phi}. \quad (2b)$$

Notice the discontinuity of the magnetic induction and the continuity of the vector potential at the boundary between the excluded and the allowed regions. In addition, the electronic wavefunctions must satisfy the boundary conditions appropriate for the quantum antidot,

$$\Psi(\rho = a, \phi, z) = 0 \quad \text{and} \quad \Psi(\rho \rightarrow \infty, \phi, z) = 0. \quad (3)$$

The solutions of the Schrödinger equation in situation A) correspond to the quantum antidot Landau states. The analysis of situation B), especially the modification of the states

relative to A) due to the presence of the additional electromagnetic vector potential term in the allowed region, Eq.(2b), leads to the characterization of the Aharonov-Bohm effect on the Landau states.

II-1. Quantum antidot Landau states

The Schrödinger equation for the electron moving in the allowed region under the action of the electromagnetic vector potential of Eq. (2a) takes the following form:

$$\left\{ -\frac{\hbar^2}{2m_e} \left[\frac{1}{\rho} \frac{\partial}{\partial \rho} \rho \frac{\partial}{\partial \rho} + \frac{\partial^2}{\partial z^2} \right] + \frac{l_z^2}{2m_e \rho^2} + \frac{eB}{2m_e c} l_z + \frac{e^2 B^2}{8m_e c^2} \rho^2 \right\} \Psi(\rho, \phi, z) = E \Psi(\rho, \phi, z), \quad (4)$$

where l_z is the z-component of the orbital angular momentum, and the last three terms in the Hamiltonian correspond to the rotational kinetic energy around the z-axis, the diamagnetic energy, and the harmonic oscillator energy with a frequency $\omega = eB/2m_e c$. Equation (4) admits separable solutions of the form

$$\Psi(\rho, \phi, z) = R(\rho)\Phi(\phi)Z(z), \quad (5)$$

in which each factor satisfies the respective ordinary differential equation:

$$l_z^2 \Phi(\phi) = m^2 \hbar^2 \Phi(\phi), \quad (6a)$$

$$-\frac{\hbar^2}{2m_e} \frac{d^2 Z(z)}{dz^2} = E^L Z(z), \quad (6b)$$

$$\left\{ -\frac{\hbar^2}{2m_e} \left[\frac{1}{\rho} \frac{d}{d\rho} \rho \frac{d}{d\rho} \right] + \frac{\hbar^2 m^2}{2m_e \rho^2} + \hbar \omega m + \frac{1}{2} m_e \omega^2 \rho^2 \right\} R(\rho) = E^T R(\rho). \quad (6c)$$

Here, $m = 0, \pm 1, \pm 2, \dots$ due to the single valuedness condition on Φ for ϕ and $\phi + 2\pi$. The superindices L and T in the energies of the Eqs. (6b) and (6c) stand for the longitudinal and transverse contributions to the total energy,

$$E = E^L + E^T. \quad (7)$$

Equations (6a) and (6b) and their solutions are well known. The longitudinal function can be chosen through the boundary conditions corresponding to free, periodic or confined motions. Next, we concentrate in the analysis of Eq. (6c) and its solutions.

Of course, it is the same equation that describes the normal Landau states when the electron has the entire space available for its motion. In such a case, the solutions correspond to the two-dimensional harmonic oscillator states,

$$R_{nm}(\rho) = N_{nm}\rho^{|m|}e^{-m_e\omega\rho^2/2\hbar}M(-n, |m| + 1, \frac{m_e\omega\rho^2}{\hbar}), \tag{8}$$

where $n = 0, 1, 2, \dots$ and $M(\alpha, \beta, z)$ is the Kummer confluent hypergeometric function of the first kind [10, 11], which for $\alpha = -n$ becomes a polynomial of degree n . The transverse energy is the sum of the harmonic oscillator energy plus the diamagnetic energy,

$$E_{nm}^T = \hbar\omega(2n + |m| + m + 1). \tag{9}$$

The normal Landau energy spectrum consists of equally spaced energy levels with a spacing of $2\hbar\omega$. Each level is infinitely degenerate due to the cancellation of the m dependent terms in Eq. (9) for $m = -|m|$. These properties are recalled here in order to use them as points of comparison in what follows.

The solutions of Eq. (6c) for the quantum antidot are subject to the boundary conditions of Eq. (3). Let us recall that, in general, the Kummer function $M(\alpha, \beta, z)$ is regular at the origin $z \rightarrow 0$, and exponentially divergent as $z \rightarrow \infty$, while the second Kummer function $U(\alpha, \beta, z)$ is singular at the origin and behaves asymptotically as $z^{-\alpha}$. These conditions and properties determine that the radial wavefunction describing the quantum antidot is

$$R_{\nu m}(\rho) = N_{\nu m}\rho^{|m|}e^{-m_e\omega\rho^2/2\hbar}U(-\nu, |m| + 1, \frac{m_e\omega\rho^2}{\hbar}). \tag{10}$$

Since the second parameter $|m| + 1$ of this Kummer function is an integer, its logarithmic representation is the appropriate one:

$$U(\alpha, n + 1, z) = \frac{(-)^{n+1}}{n!\Gamma(\alpha - n)}[M(\alpha, n + 1, z)\ln z + \sum_{r=0}^{\infty} \frac{(\alpha)_r z^r}{(n + 1)_r r!} \{\psi(\alpha + r) - \psi(1 + r) - \psi(1 + n + r)\}] + \frac{(n - 1)!}{\Gamma(\alpha)} z^{-n} M(\alpha - n, 1 - n, z)_n, \tag{11}$$

for $n = 0, 1, 2, \dots$, where $\psi(x) = \Gamma'(x)/\Gamma(x)$, and the last factor is the sum of n terms with the value zero for $n = 0$ [10, 11].

The correct asymptotic behavior of Eq.(3) is obviously satisfied, and the other boundary condition becomes

$$U(-\nu, |m| + 1, \frac{m_e\omega a^2}{\hbar}) = 0. \tag{12}$$

The solution of this equation for the parameter ν determines the energy eigenvalues of the quantum antidot:

$$E_{sm}^T = \hbar\omega(2\nu_s + |m| + m + 1). \quad (13)$$

The reader may appreciate the difference between the eigenfunctions and energy eigenvalues of the Landau levels of the quantum antidot and of the electron in all space. The change from equations (8) to (10) consists in the replacement of the first Kummer function by the second one, while the corresponding change from Eq.(9) to (13) is the replacing of the integer n by the parameter ν_s for the successive roots $s = 1, 2, 3, \dots$ from Eq. (12). The energy levels of Eq. (13) are not equally spaced, but do exhibit infinite quasi-degeneracy due to the same cancellation of their m dependent terms for $m = -|m|$ as in Eq. (9).

II-2. Aharonov-Bohm effect in the Landau states

The Schrödinger equation for the quantum antidot under the action of the electromagnetic vector potential of Eq. (2b) is

$$\left\{ -\frac{\hbar^2}{2m_e} \left[\frac{1}{\rho} \frac{\partial}{\partial \rho} \rho \frac{\partial}{\partial \rho} + \frac{\partial^2}{\partial z^2} \right] + \frac{(l_z + \frac{eB_d a^2}{2c})^2}{2m_e \rho^2} + \frac{eB}{2m_e c} (l_z + \frac{eB_d a^2}{2c}) + \frac{e^2 B^2}{8m_e c^2} \rho^2 \right\} \Psi(\rho, \phi, z) = E \Psi(\rho, \phi, z). \quad (14)$$

A comparison with Eq. (4) shows that the difference resides in the term added to the l_z operator, which arises from the extra term in the potential of Eq. (2b), due to the difference, $B_d = B' - B$, between the magnetic induction fields in the excluded and the allowed regions. It is convenient to rewrite

$$\frac{eB_d a^2}{2c} = \hbar \frac{\pi a^2 B_d}{(\frac{hc}{e})} = \hbar \mu \quad (15)$$

in terms of the difference of magnetic flux in the excluded region in situations B) and A), expressed in the natural unit hc/e . Equation (14) also admits a separable solution as in Eq. (5), with the same ϕ and z dependent functions, and a radial function which satisfies the equation

$$\left\{ -\frac{\hbar^2}{2m_e} \left[\frac{1}{\rho} \frac{d}{d\rho} \rho \frac{d}{d\rho} \right] + \frac{\hbar^2(m + \mu)^2}{2m_e \rho^2} + \hbar\omega(m + \mu) + \frac{1}{2} m_e \omega^2 \rho^2 \right\} R(\rho) = E^T R(\rho), \quad (16)$$

The difference between Eqs. (16) and (6c) consists in the substitution of m by $m + \mu$, involving the difference of the magnetic fluxes between A) and B) and affecting the rotational kinetic energy around the z -axis and the diamagnetic energy terms. Equation (16) is a radial harmonic oscillator Schrödinger equation and its eigensolutions for the quantum antidot can be written as

$$R_{\nu m}(\rho; \mu) = N_{\nu m} \rho^{|m+\mu|} e^{-m_e \omega \rho^2 / 2\hbar} U(-\nu, |m + \mu| + 1, \frac{m_e \omega \rho^2}{\hbar}). \quad (17)$$

Its energy eigenvalues are

$$E_{sm}^T(\mu) = \hbar \omega (2\nu_s + |m + \mu| + m + \mu + 1), \quad (18)$$

where the parameter ν_s , $s = 1, 2, 3, \dots$ follows from the boundary condition

$$U(-\nu, |m + \mu| + 1, \frac{m_e \omega a^2}{\hbar}) = 0. \quad (19)$$

Since now the second parameter $|m + \mu| + 1$ of the U Kummer function is in general not an integer, the appropriate representation [10, 11] is

$$U(\alpha, \beta, z) = \frac{\pi}{\sin \pi \beta} \left(\frac{M(\alpha, \beta, z)}{\Gamma(1 + \alpha - \beta)\Gamma(\beta)} - z^{1-\beta} \frac{M(1 + \alpha - \beta, 2 - \beta, z)}{\Gamma(\alpha)\Gamma(2 - \beta)} \right). \quad (20)$$

III. NUMERICAL RESULTS AND DISCUSSION

The quantum antidot was defined in section II via the radius a of the cylindrical region from which the electron is excluded. Its Landau states were analyzed in section II.1 and are described by the radial eigenfunctions of Eqs. (10) and (11) and the energy eigenvalues of Eq. (13), as determined by the roots of the boundary condition of Eq. (12). An analysis of the Aharonov–Bohm effect on the quantum antidot Landau states was carried out in section II.2 with the corresponding eigenfunctions of Eqs. (17) and (20), the eigenenergies of Eq. (18) and the boundary condition of Eq. (19), where their dependence on the magnetic flux difference in the excluded region, Eq. (15), is the important feature. Numerical solutions of the equations for both problems were obtained by using the routines from [11], which are now presented and discussed, for quantum antidots with radius a for the chosen values of the arguments of Eqs. (12) and (19), $m_e \omega a^2 / \hbar = 0.01, 0.1, 1$ and 10 .

Results illustrative of the anticonfinement effect of the electron on its Landau states are presented in Table I and Fig. 1. The chosen values for the radius correspond to small, medium, and large excluded regions for the electron, respectively. The departure of the transverse energy eigenvalues of the Landau states for the quantum antidot E_{sm}^T , Eq. (13),

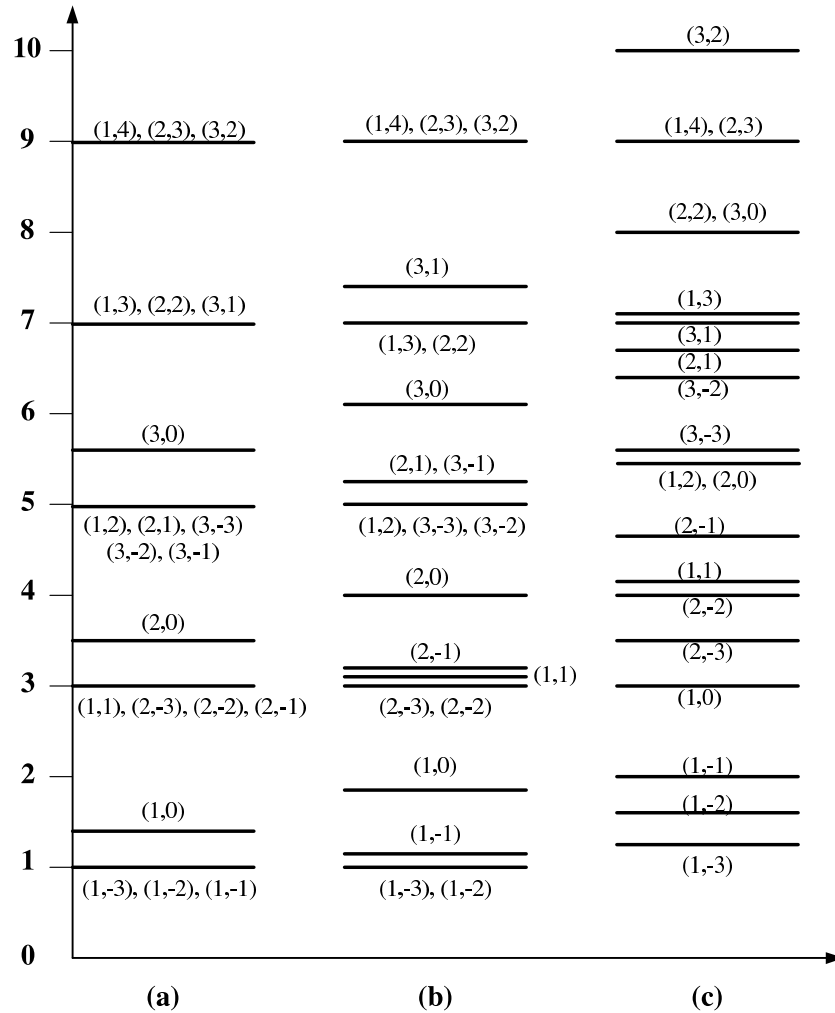


FIG. 1: Transverse energy spectra E_{sm}^T , Eq.(13), of Landau states for quantum antidots with radius a such that $m_e \omega a^2 / \hbar$ equals: a) 0.01, b) 0.1, and c) 1.

from the normal ones E_{nm}^T , Eq. (9), with $s = n+1$, is a measure of the anticonfinement effect on the Landau-state energy spectra. States when $n = 0$ are the most affected, because in a normal situation the electron has a large probability of being found in the $0 < \rho < a$ region, Eq. (8), from which it is excluded in the quantum antidot. The effect is considerably reduced as $|m|$ takes increasingly larger values. On the other hand, the effect becomes smaller or larger according to the size of the excluded region. The reader can check these general trends by looking at the entries in Table I in the order of increasing angular momentum $|m| = 0, 1, 2, \dots$, radial $s = 1, 2, 3, \dots$ excitations, and radius a , comparing them with the odd integer

TABLE I: Lower transverse energy eigenvalues $E_{sm}^T/\hbar\omega$ Eq. (13) of quantum antidot Landau states as functions of the antidot radius a (for given values of $m_e\omega a^2/\hbar$), angular momentum m and radial excitation s .

$m_e\omega a^2/\hbar$	0.01			0.1			1		
m	$s = 1$	2	3	1	2	3	1	2	3
-3	1.0000	3.0000	5.0000	1.0095	3.0032	5.0095	1.2441	3.5271	5.8005
-2	1.0002	3.0006	5.0011	1.0164	3.0431	5.0762	1.5769	4.0044	6.3594
-1	1.0192	3.0371	5.0541	1.1655	3.2890	5.3931	2.1479	4.6845	7.0933
0	1.4486	3.5328	5.5897	1.8003	4.0026	6.1477	3.0000	5.5769	8.0044
1	3.0192	5.0371	7.0541	3.1655	5.2890	7.3931	4.1479	6.6845	9.0933
2	5.0002	7.0006	9.0011	5.0164	7.0431	9.0762	5.5769	8.0044	10.0921
3	7.0000	9.0000	11.0000	7.0009	9.0032	11.0073	7.2441	9.5271	11.8005
4	9.0000	11.0000	13.0000	9.0000	11.0001	13.0004	9.0835	11.2321	13.4107
5	11.0000	13.0000	15.0000	11.0000	13.0000	15.0000	11.0225	13.0817	15.1745

values $2N + 1$ of the normal Landau states Eq. (9). Figure 1 shows the lower energy spectra for the respective quantum antidot. For a small radius the quasi-degeneracy of the states with $m \neq 0$ at the normal Landau-state eigenenergies is immediately apparent, and the anticonfinement effect is restricted to the upward shift of the $(s, m = 0)$ states; these results are numerically manifested through the near equalities of ν_s and n and the inequalities $\nu_s > n$, of the respective solutions for Eq. (12). For a larger radius quantum antidot, these inequalities become larger and extend to states with $|m| = 1, 2, \dots$, as manifested by the successive upward and increasingly larger shifts of the (sm) energy levels when going from a) to b) and then to c), as in Figure 1. The specific numerical results of our calculations have been restricted to the reported finite values of a, m , and s , which is enough for one to recognize and identify the general and specific trends discussed above. Of course they also serve for extrapolation to what can be expected when larger values of $|m|$ and s are included. In particular, for a given value of a , it is possible to go to large enough values of $|m|$ for which the near equality of ν_s and n holds and the Landau states quasi-degeneracy is exhibited, while the states with lower $|m|$ values are associated with the inequalities $\nu_s > n$ and are shifted upwards, exhibiting the anticonfinement effect on the Landau states.

The numerical results that illustrate the Aharonov-Bohm effect on the quantum antidot Landau states are contained in Table II and Fig. 2. Table II is restricted to medium size quantum antidots and to Landau states without radial excitation ($s = 1$) and angular momentum $m = -3, -2, -1, 0, 1, 2, 3$. It presents the energies $E_{1m}^T(\mu)$, Eq. (18), for values of the magnetic flux difference μ , Eq. (15), from -1 to 1 in steps of 0.2 . The reader can check that the entries in the middle row for $\mu = 0$ coincide with the corresponding ones of the quantum antidot Landau states with $s = 1$ given in the fourth column of Table I. The Aharonov-Bohm effect is exhibited through the dependence of the energy eigenvalues on the magnetic flux difference, which can be read from the entries along each column in Table II. When going from section II.1 to section II.2 it was recognized that the Aharonov-Bohm

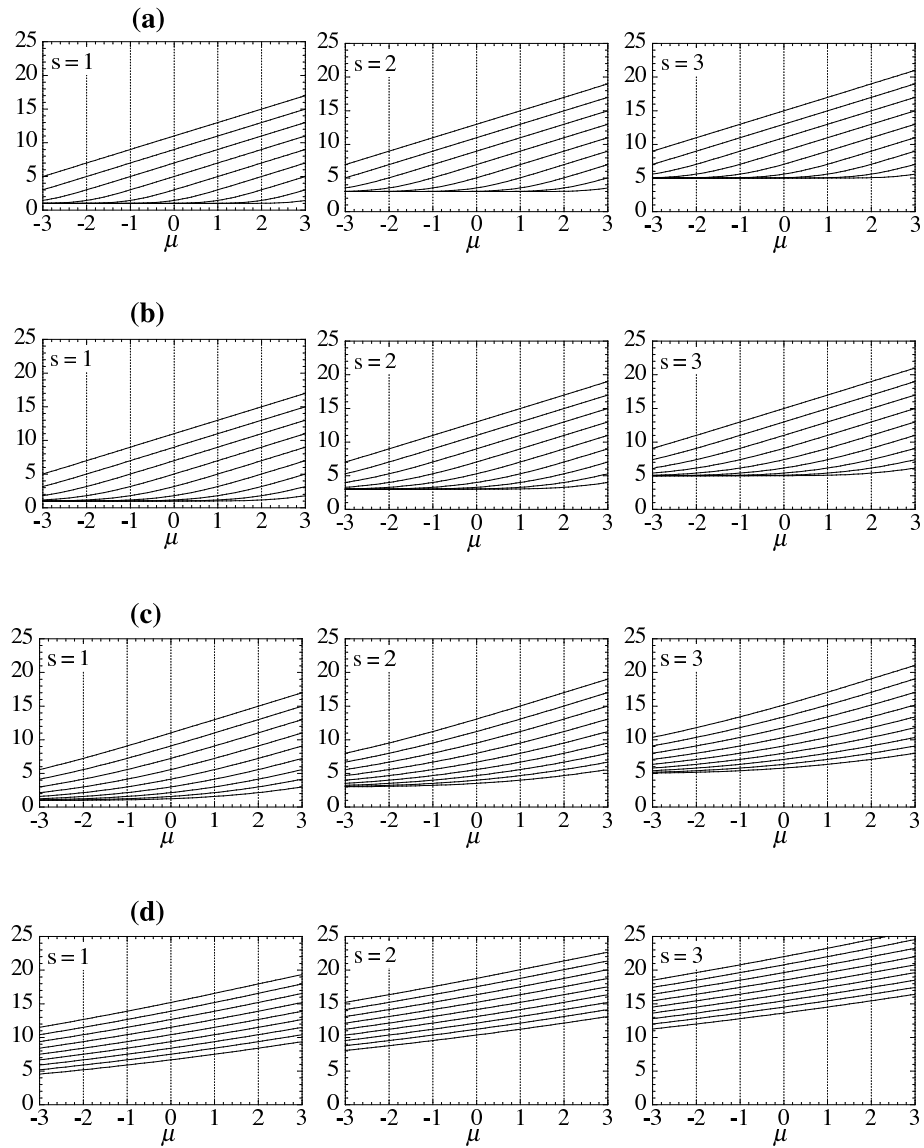


FIG. 2: Aharonov–Bohm effect on Landau states $E_{sm}^T(\mu)$, Eq. (18), with $s = 1, 2, 3$ and $m = -3, -2, -1, 0, 1, 2, 3, 4, 5$ (from bottom to top) as functions of the magnetic flux difference μ for quantum antidots with radius a such that $m_e \omega a^2 / \hbar$ equals: a) 0.01, b) 0.1, c) 1.0 and d) 10.

equations differ from those of the original situation by the replacement of $m \rightarrow m + \mu$, as appreciated when comparing the differential Eqs. (16) and (6c), the radial eigenfunctions of Eqs. (17) and (10), the energy eigenvalues Eqs. (18) and (13), and the boundary condition Eqs. (19) and (12). The roots ν_s of the latter depend only on the value of the combination $m + \mu = (m - 1) + (\mu + 1) = \dots = (m - N) + (\mu + N)$ for $N = 0, \pm 1, \pm 2, \dots$ leading to the

TABLE II: Transverse energy eigenvalue $E_{lm}^T/\hbar\omega$ of Landau states without radial excitation ($s = 1$) and different angular momentum m as functions of the magnetic flux difference μ for quantum antidots with radius a , such that $m_e\omega a^2/\hbar = 0.1$.

μ	$m = -3$	-2	-1	0	1	2	3
1.0	1.0164	1.1655	1.8003	3.1655	5.0164	7.0009	9.0000
0.8	1.0095	1.1107	1.6159	2.8400	4.6276	6.6016	8.6001
0.6	1.0054	1.0718	1.4623	2.5378	4.2452	6.2030	8.2001
0.4	1.0030	1.0452	1.3378	2.2623	3.8718	5.8054	7.8002
0.2	1.0016	1.0276	1.2400	2.0159	3.5107	5.4095	7.4005
0.0	1.0009	1.0164	1.1655	1.8003	3.1655	5.0164	7.0009
-0.2	1.0005	1.0095	1.1107	1.6159	2.8400	4.6276	6.6016
-0.4	1.0002	1.0054	1.0718	1.4623	2.5378	4.2452	6.2030
-0.6	1.0001	1.0030	1.0452	1.3378	2.2623	3.8718	5.8054
-0.8	1.0001	1.0016	1.0276	1.2400	2.0159	3.5107	5.4095
-1.0	1.0000	1.0009	1.0164	1.1655	1.8003	3.1655	5.0164

equality of the energy eigenvalues

$$E_{sm}^T(\mu) = E_{s,m-1}(\mu + 1) = \dots = E_{s,m-N}(\mu + N), \quad (21)$$

which translates into the periodic repetition of the energy spectrum when the magnetic flux density is changed by one unit, with the compensating change of one unit in the angular momentum of the eigenstate. The reader can check this periodicity in Table II by noting the coincidence of the entries in the upper half of each column with those in the lower half in the neighboring column on the right. Figure 2 shows graphically the Aharonov-Bohm effect on Landau states $E_{sm}^T(\mu)$ with lower radial $s = 1, 2, 3, \dots$ and angular momentum $m = -3, -2, -1, 0, 1, 2, 3, 4, 5$ (from bottom to top) excitations as the magnetic flux difference μ is changed between -3 and 3 for: a) small, b) medium, c) large, and d) very large radius quantum antidots. In all cases the energy eigenvalues show a monotonic increase as the magnetic flux difference μ increases. For $s = 1, 2, 3$ the lower eigenvalues start from the normal Landau state degenerate values of 1, 3, and 5 as explicitly shown in a), b), and c). The same trend will appear for d) when large values of $|m|$ are included, as has already been discussed at the end of the previous paragraph. The energy curves for each given radius a , each radial excitation, and different angular momentum values have the same shape and differ only in their positions which correspond to one unit shifts to the right or to the left, in agreement with Eq. (21) and the periodicity of the energy spectrum characteristic of the Aharonov-Bohm effect. It is also clear that, if the graphs are extended to include additional positive and negative values of μ , the shape of each energy curve is asymptotically horizontal to the left and increases monotonically to the right; correspondingly, each set of curves becomes degenerate to the left and the spacing between them tends to $2\hbar\omega$ to the right, reminding us of their Landau nature.

We conclude this section by pointing out some connections between the models of the present work, the annular box [4], and the two-dimensional ring [7]. The quantum antidot is the limiting case of the annular box when the upper, lower and outer walls are sent to infinity [4]. The longitudinal motion of the quantum antidot described by Eq. (6b) must be eliminated in order to connect with the two-dimensional model of [7], in which the harmonic oscillator confining potential must also be eliminated. The presence of the inner and outer walls in [4] translates into the corresponding boundary conditions, which requires the use of both Kummer functions in the transverse radial eigenfunctions. The removal of the outer wall in the quantum antidot translates into the removal of the Kummer function of the first kind from the corresponding radial eigenfunction, Eq. (10). In contrast, the model of [7] uses a radial eigenfunction with a Kummer function of the first kind only, like that of Eq. (8), except for the substitution of the angular momentum m by the effective centrifugal potential parameter, which includes contributions from the rotational kinetic energy, and the centrifugal potential which models the exclusion of the electron from the central region. The interested reader may compare Figs. 2 of [4] and the present work to appreciate the differences in the energy curves $E_{sm}^T(\mu)$ illustrating the Aharonov-Bohm effect on the Landau states, for the respective confinement situations. While the exclusion of the electron from the central region leads to energy curves $E_{sm}^T(\mu)$ that increase monotonically as μ increases, as discussed in the previous paragraph, the confining effect of the outer wall in [4] leads to a corresponding monotonic increase as μ decreases, with the result that energy curves for the annular box have one minimum in the interval $-1 - m < \mu < -m$. As the outer wall is moved to infinity the monotonic increase of the energy curves on the left side is reduced, so that in the limit of the quantum antidot they become asymptotically horizontal and infinitely quasi-degenerate, as illustrated in Fig. 2. Finally, Tan and Inkson have applied their model to investigate the magnetization, persistent currents, and their relation to quantum rings and dots [12]. Similar investigations are worth doing on the basis of the models of [4] and this work.

References

- * Electronic address: naa@xanum.uam.mx
- † Electronic address: ele@xanum.uam.mx
- ‡ Electronic address: eleykoo@fisica.unam.mx
- [1] L. D. Landau, *Z. Phys.* **64**, 629 (1930).
- [2] L. D. Landau and I. M. Lifshits, *Quantum Mechanics*, (Pergamon Press, Oxford, 1977).
- [3] M. K. Fung and Y. F. Wang, *Chin. J. Phys.* **37**, 435 (1999).
- [4] E. Ley-Koo, G. Villa-Torres and D. Kouznetsov, *Chin. J. Phys.* **40**, 130 (2002).
- [5] R. A. Weeb, Washburn, S., *Adv. Phys.* **35**, 375 (1986); S. Datta, *Electronic transport in mesoscopic systems*, (Cambridge University Press, Cambridge, 1989); C. W. J. Beenakker, and H. van Houten, *Quantum transport in semiconductor nanostructures*, in *Solid State Physics*, Ed. H. Eherenreich and D. Turnbull, (Academic Press, San Francisco, 1991), **44**, 1-228; Y. Imry, *Introduction to mesoscopic physics*, (Oxford University Press, Oxford 1997); D. K. Ferry, S. M. Goodnick, *Transport in nanostructures*, (Cambridge University Press, Cambridge 1997); J.

- H. Davis, *The physics of low dimensional systems: an introduction*, (Cambridge University press, Cambridge 1997); *Low - Dimensional semiconductor structures: Fundamentals and device applications*, eds. K. Barnham, D. Vvedensky, (Cambridge University Press, Cambridge 2001).
- [6] L. P. Kouwenhoven, D. G. Austing and S. Tarucha, Rep. Prog. Phys. **64**, 701 (2001).
 - [7] W. C. Tan and J. C. Inkson, Semicond. Sci. Technol. **11**, 1635 (1996).
 - [8] Y. Aharonov and D. Bohm, Phys. Rev. **115**, 485 (1959).
 - [9] R. G. Chambers, Phys. Rev. Lett. **5**, 3 (1960).
 - [10] M. Abramowitz and I. A. Stegun, *Handbook of Mathematical Functions*, (Dover Publications, Inc. New York, 1965) Chap. 13.
 - [11] S. Zhang and J. Jin, *Computation of Special Functions*, (John Wiley and Sons, Inc. New York 1996).
 - [12] W. C. Tan and J. C. Inkson, Phys. Rev. B **60**, 5626 (1999).